Gala Wind
3/29/2011

Analysis of differences between Science Test 8B and 8D

In this document we illustrate the differences in results between science tests 8B and 8D. Science test(ST) 8B is the baseline test. We skip science test 8C, as it was a bug fix for the 1-km McGarrah cloud top properties MOD_PR06CT code and there were no changes to the optical properties code. Science test 8D shows changes due to use of land surface emissivity database for 3.7 μm surface albedo instead of setting the 3.7 μm land surface albedo to be ½ of the 2.1 μm one. This change of course affects the 3.7 μm retrievals only. Another change that we've inserted is use of spatially and temporally interpolated column ozone from GDAS as opposed to using the TOAST daily column ozone product values in nearest-neighbor lookup. This change affects retrievals over land only and mainly concerns the retrieval of cloud optical thickness. We also added some significant optimizations on library interpolation and were able to increase the amount of interpolation we do while actually decreasing the total execution time. This led to appearance of a number of newly successful retrievals over ocean.

We have examined impacts of these changes in the science test for one-month duration for April 2005, Terra and Aqua MODIS. Global images of means and differences between tests for a wide variety of parameters are available at:

http://modis-atmos.gsfc.nasa.gov/team/pge06_test_details.html

under the heading of Science Test 8D.

Figure 1 shows global maps of TOAST and GDAS 6-hourly total column ozone in DU. Figure 1a shows the TOAST product, a single file that would've been used to process the entire day of April 1st, 2005. The rest of the panels show the GDAS 6-hourly fields. For Science Test 8D we temporally and spatially interpolate those fields.

Next we looked in detail at areas where patterns exist such that changes implemented for this test would be most visible. We examined two cases. The first one is an area over the Western US, the same area that we used for the ST8B-ST8A assessment. This case has a frontal system present and shows a strong gradient of ozone amount. Figure 2 shows the RGB image, the total ozone, and 3.7 μm surface albedo fields. The position of features in the total ozone content is quite different between GDAS and TOAST. The tongue of low ozone, likely corresponding to tropical air getting pulled

north ahead of the cold front, is shifted west in the TOAST product and seems to be more in line with the cloud features in the GDAS product. It is hard to make any significant judgments on the 3.7 μm surface albedo as the two come from completely different sources and are just different. The emissivity-derived albedo used in ST8D is generally lower than the original MOD43-extrapolated one, which would lead to smaller 3.7 μm effective radii being retrieved as more radiation would make it into the solar signal.

Figures 3-5 show the retrieval results and differences for Terra MODIS 2005 day 091 18:15UTC. Figures 6-8 show retrieval results and differences for Aqua MODIS 2005 day 091 at 19:55 UTC. Figure 9 shows histograms for ice and liquid water phase retrievals of cloud optical and microphysical properties taken in a lat/lon box (UL,LR: (56°,-125°), (40°, -100°)). Tables 1 and 2 show changes in retrieval means within indicated boxes. Both Terra and Aqua show similar minor impacts with mean optical thickness increasing by between 0.14 and 0.6 unit, which is about +7% change at the maximum impact. The 1.6 and 2.1 μm effective radius retrievals also changed slightly because of change in optical thickness, but the differences are with the emphasis on 'slightly' as the maximum change in the retrieval is +0.12 μm, which translates into ~0.65%, a rather negligible amount. The 3.7 μm retrieval decreased as predicted mainly due to lower surface albedo, by about a μm for ice clouds and 0.5 μm for liquid water clouds. Even though the mean cloud optical thickness would indicate otherwise, the histograms show that the ice clouds in this scene are generally thinner and so would be more impacted by changes in surface albedo.

The second case we examined also shows a great deal of ice cloud over the northern Arabian Sea. We have Terra MODIS 2005, day 111 at 06:25UTC and Aqua MODIS at 09:30UTC. Figure 10 shows a comparison of ancillary fields used in tests 8B and 8D. Figures 11-13 show retrievals and differences for Terra overpass and Figures 14-16 show the Aqua overpass. Figure 17 show the histograms taken in a lat/lon box (UL,LR: (32°, 56°), (16°, 72°)).

In this case the impact due to different column ozone amounts is quite small and the main retrievals indicate so with changes of <0.1 unit in optical thickness and <0.1 μm in effective radius from 1.6 and 2.1 μm. The 3.7 μm retrievals show the impact of different surface albedo as an overall decrease in the retrieval because in this case emissivity-derived land surface albedo is lower than the MOD43-derived one. The 3.7 μm

histograms, like the ones for the Western US, show mostly a uniform left shift, although not as pronounced.

In this document we outlined retrieval changes that resulted from substitution of a land surface emissivity database for 3.7 μm surface albedo from UW-Madison and spatially and temporally interpolated column ozone amount from GDAS. We show global monthly statistics and an in-depth look at a couple of interesting cases. Overall the results of these changes is somewhat mixed. There were some minor changes to the optical thickness and 1.6 and 2.1 μm effective radius retrievals, mostly on the order of about a μm locally for radius and no more than 2 units of optical thickness. The yearly mean land surface emissivity database tends to give somewhat lower surface albedo than we used previously, thereby resulting in smaller 3.7 μm effective radius retrievals with the consequence that of course some 3.7 μm retrievals will fail. The impact of changing total column ozone map has not been great as the amount of ozone absorption in 0.65 μm is relatively small. Retrievals of optical thickness either increased or decreased somewhat locally depending on the changes in ozone distribution. The impacts on 3.7 μm retrievals was dominated by changes in surface albedo.

Case / lat,lon (UL) – (LR)	Phase	8B		8D		8D-8B	
		τ_c	$r_{e(1.6\mu m)}$	τ_c	$r_{e(1.6\mu m)}$	τ_c	$r_{e(1.6\mu m)}$
T 2005.091.1815 (56°, -125°) – (40°, -100°)	Ice	8.85	27.23	9.00	27.25	+0.15	+0.02
	Liquid	8.58	18.42	9.18	18.54	+0.6	+0.12
A 2005.091.1955 (56°, -125°) – (40°, -100°)	Ice	8.62	25.35	8.76	25.35	+0.14	0
	Liquid	9.01	18.38	9.28	18.42	+0.27	+0.04
T 2005.111.0625 (32°, 56°) – (16°, 72°)	Ice	5.13	30.07	5.09	29.95	-0.04	-0.12
	Liquid	3.04	15.30	3.04	15.41	0	+0.11
A 2005.111.0930	Ice	7.36	30.99	7.37	30.97	+0.01	-0.02
	Liquid	4.60	13.46	4.61	13.43	+0.01	-0.03

Table 1: Mean values of optical thickness and 1.6 μm cloud effective radius for all cases analyzed within box areas indicated for each granule.

Case / lat,lon (UL) – (LR)	Phase	8B		8D		8D-8B	
		$r_{e(2.1\mu m)}$	$r_{e(3.7\mu m)}$	$r_{e(2.1\mu m)}$	$r_{e(3.7\mu m)}$	$r_{e(2.1\mu m)}$	$r_{e(3.7\mu m)}$
T 2005.091.1815 (56°, -125°) – (40°, -100°)	Ice	25.23	24.05	25.24	22.71	+0.01	-1.34
	Liquid	18.26	16.56	18.34	16.05	+0.08	-0.51
A 2005.091.1955 (56°, -125°) – (40°, -100°)	Ice	22.53	21.88	22.51	20.85	-0.02	-1.03
	Liquid	15.45	15.12	15.48	14.64	+0.03	-0.48
T 2005.111.0625 (32°, 56°) – (16°, 72°)	Ice	29.59	28.38	29.5	28.2	-0.09	-0.18
	Liquid	14.21	14.67	14.30	14.38	+0.09	-0.29
A 2005.111.0930 (32°, 56°) – (16°, 72°)	Ice	28.73	31.29	28.73	31.26	0	-0.03
	Liquid	12.36	13.30	12.34	13.28	-0.02	-0.02

Table 2: Mean values of 2.1 and 3.7 μm cloud effective radius for all cases analyzed within box areas indicated for each granule.

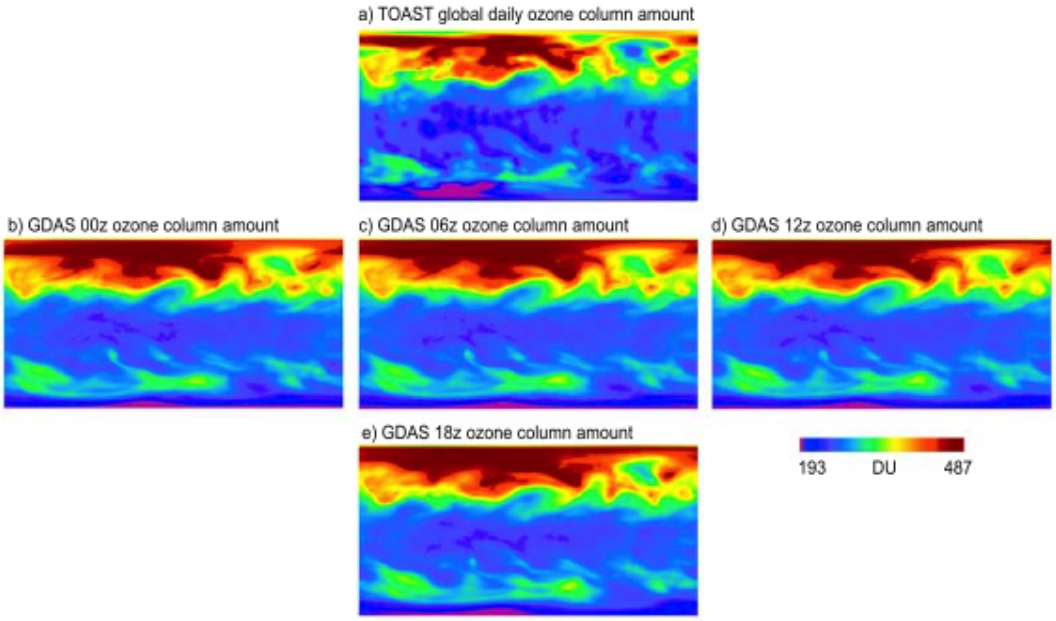

Figure 1: Global column ozone maps from GDAS and TOAST for April 1, 2005.

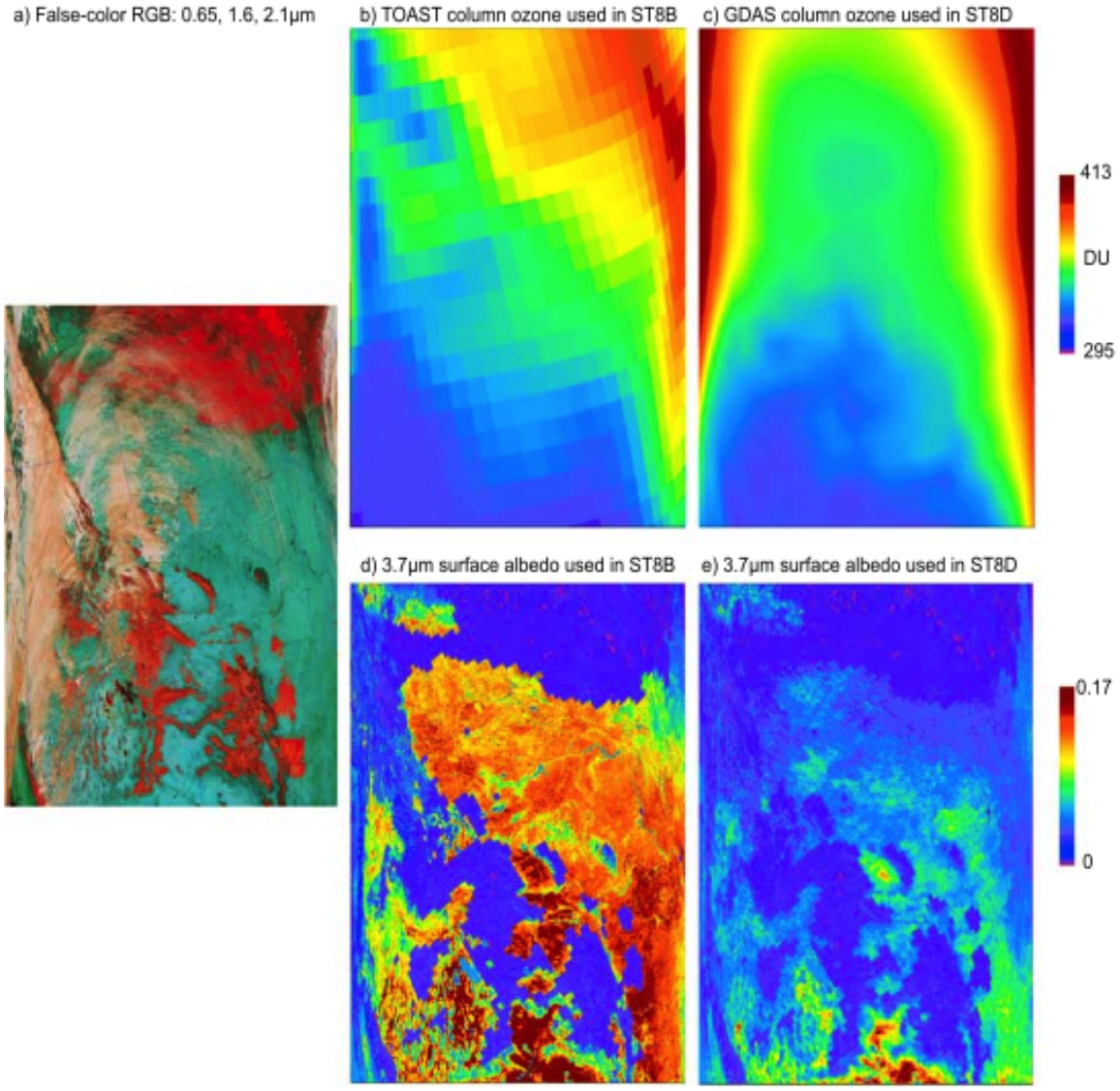

Figure 2: Terra MODIS 2005 day 091, 18:15 UTC. Panel a) shows the false-color RGB composite RGB: 0.65, 1.6, 2.1 μm. Panel b) shows the original column ozone field used in ST8B. Panel c) shows the new interpolated column ozone field. Panels d) and e) show 3.7 μm surface albedo for ST8B and ST8D respectively.

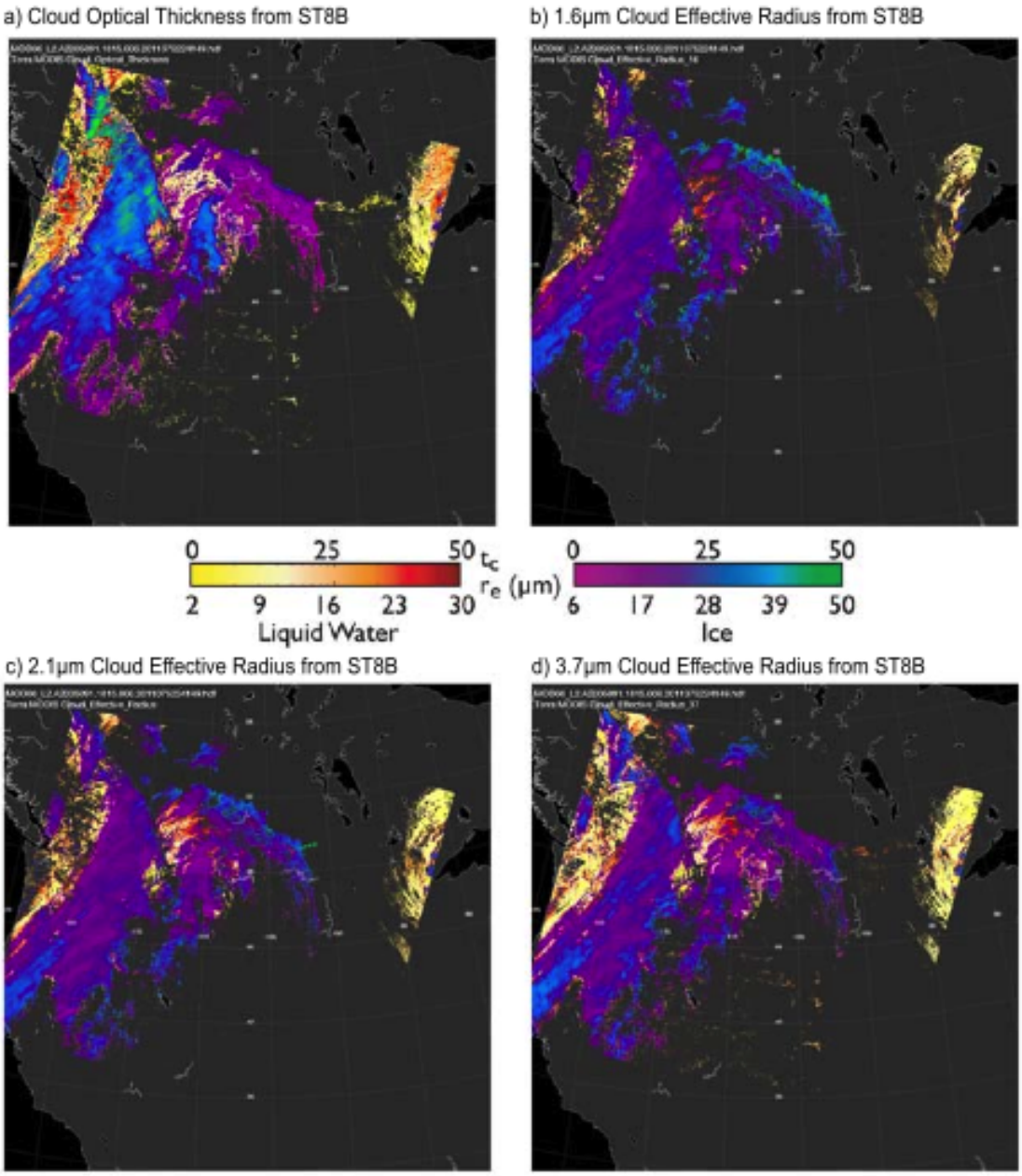

Figure 3: Terra MODIS 2005 day 091, 18:15 UTC, Western United States. The panels illustrate baseline retrievals from ST8B as cloud optical thickness in panel a), 1.6 μm cloud effective radius in panel b), 2.1 μm cloud effective radius in panel c) and 3.7 μm cloud effective radius in panel d).

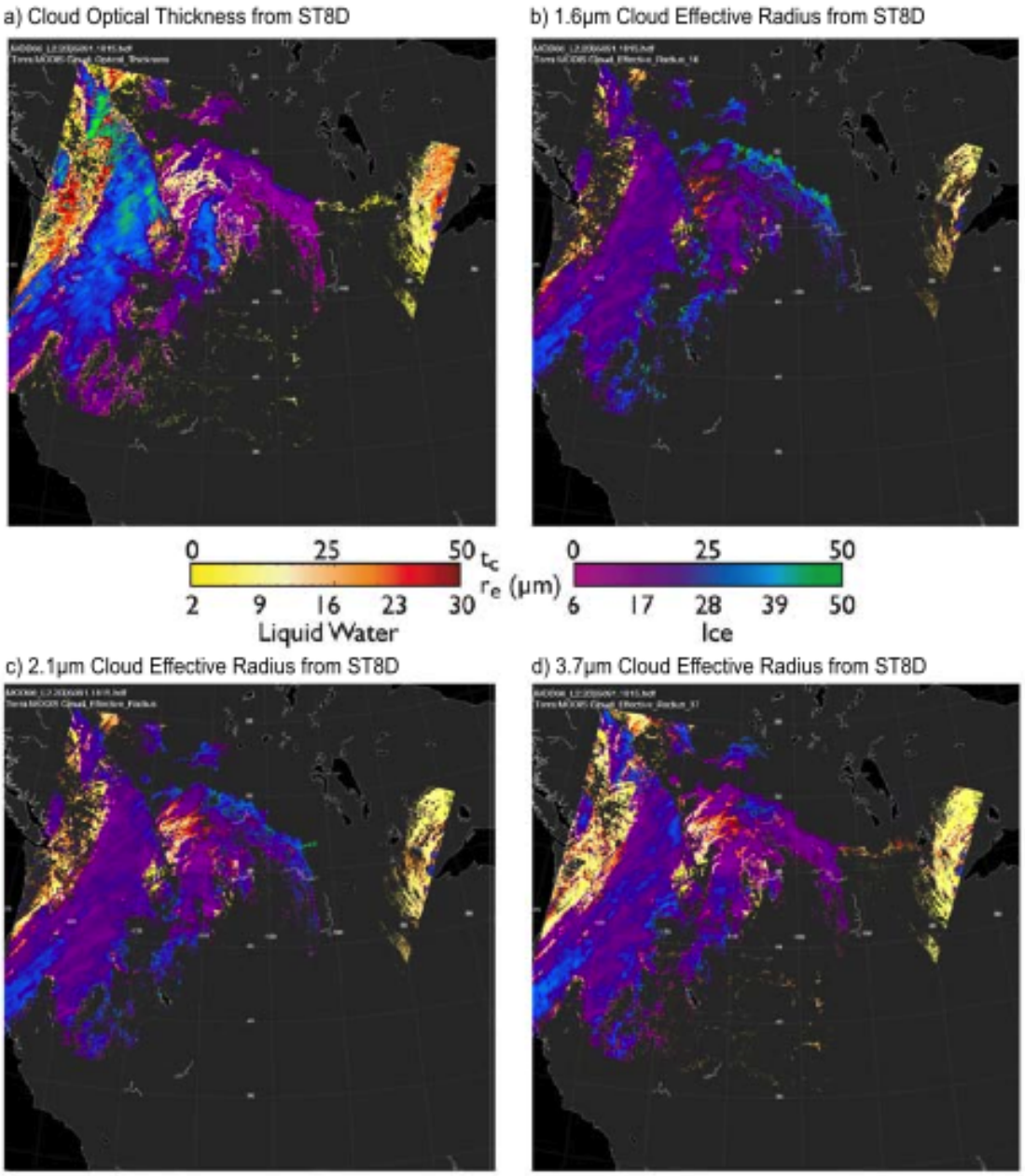

Figure 4: Terra MODIS 2005 day 091, 18:15 UTC, Western United States. The panels illustrate new retrievals from ST8D as cloud optical thickness in panel a), 1.6 μm cloud effective radius in panel b), 2.1 μm cloud effective radius in panel c) and 3.7 μm cloud effective radius in panel d).

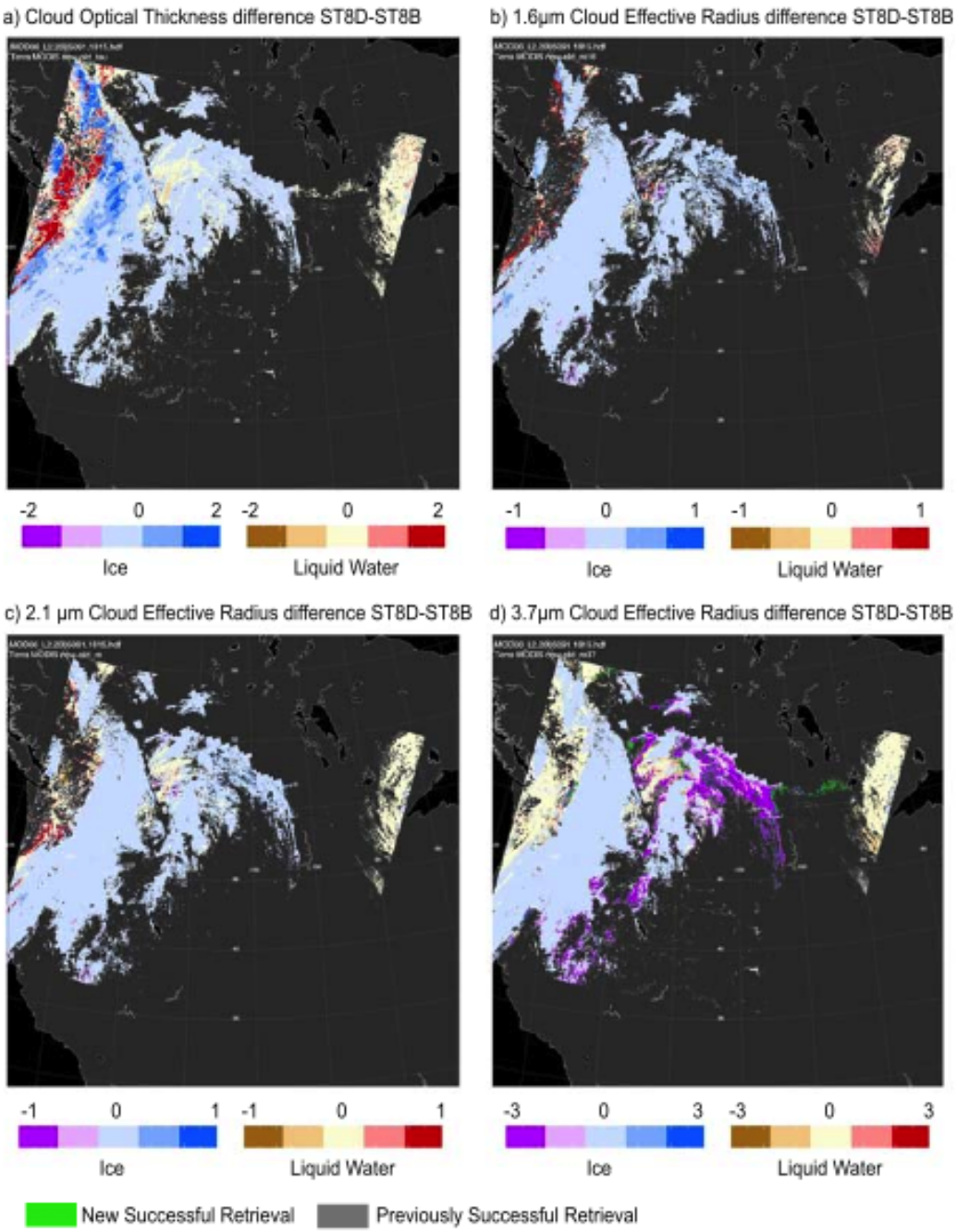

Figure 5: Terra MODIS 2005 day 091, 18:15 UTC, Western United States. The panels illustrate differences between ST8D and ST8B as cloud optical thickness in panel a), 1.6 μm cloud effective radius in panel b), 2.1 μm cloud effective radius in panel c) and 3.7 μm cloud effective radius in panel d). New successful retrievals are shown in green and retrievals that previously succeeded but now fail are in medium gray.

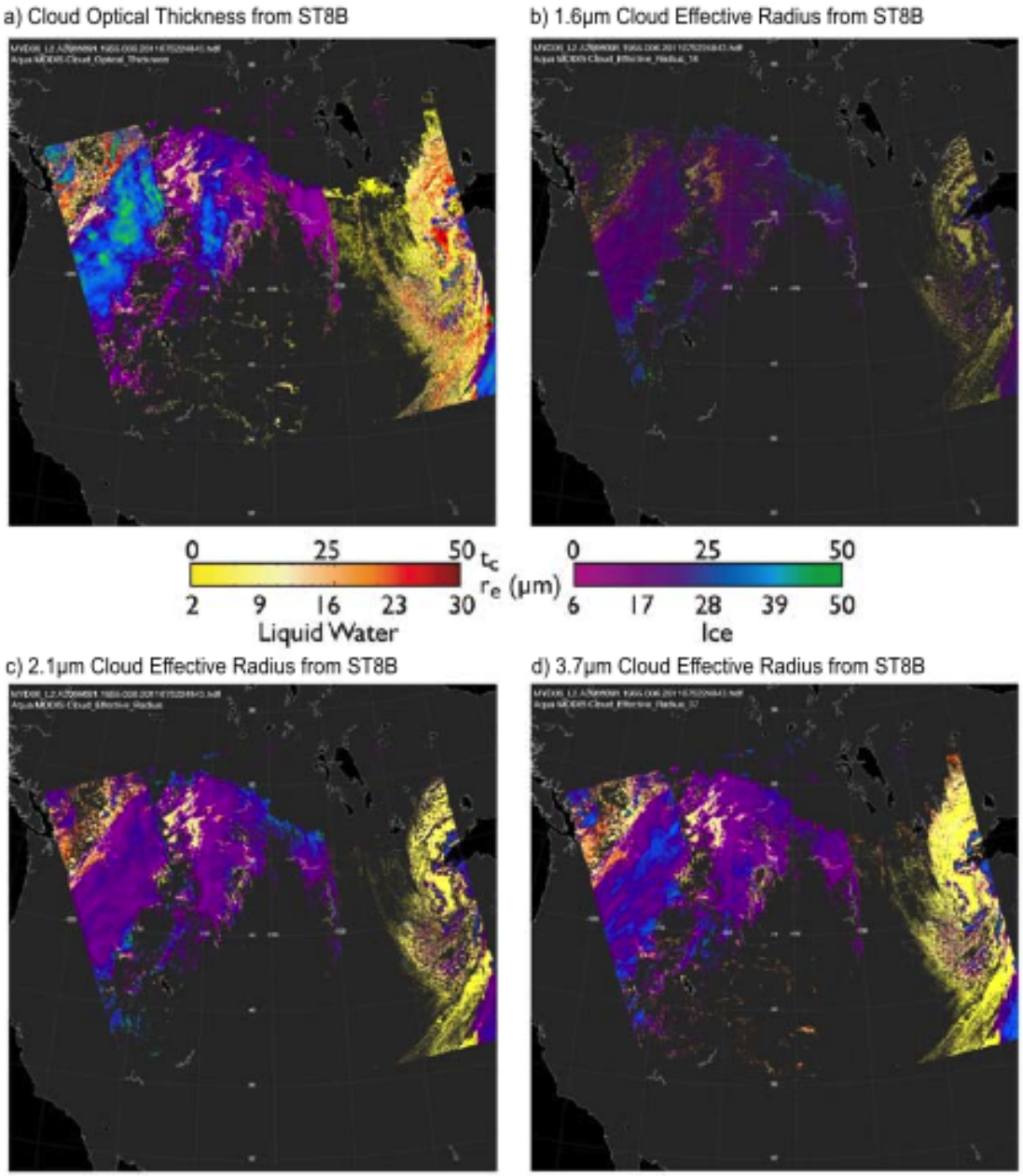

Figure 6: Aqua MODIS 2005 day 091, 19:55 UTC, Western United States. The panels illustrate baseline retrievals from ST8B as cloud optical thickness in panel a), 1.6 μm cloud effective radius in panel b), 2.1 μm cloud effective radius in panel c) and 3.7 μm cloud effective radius in panel d).

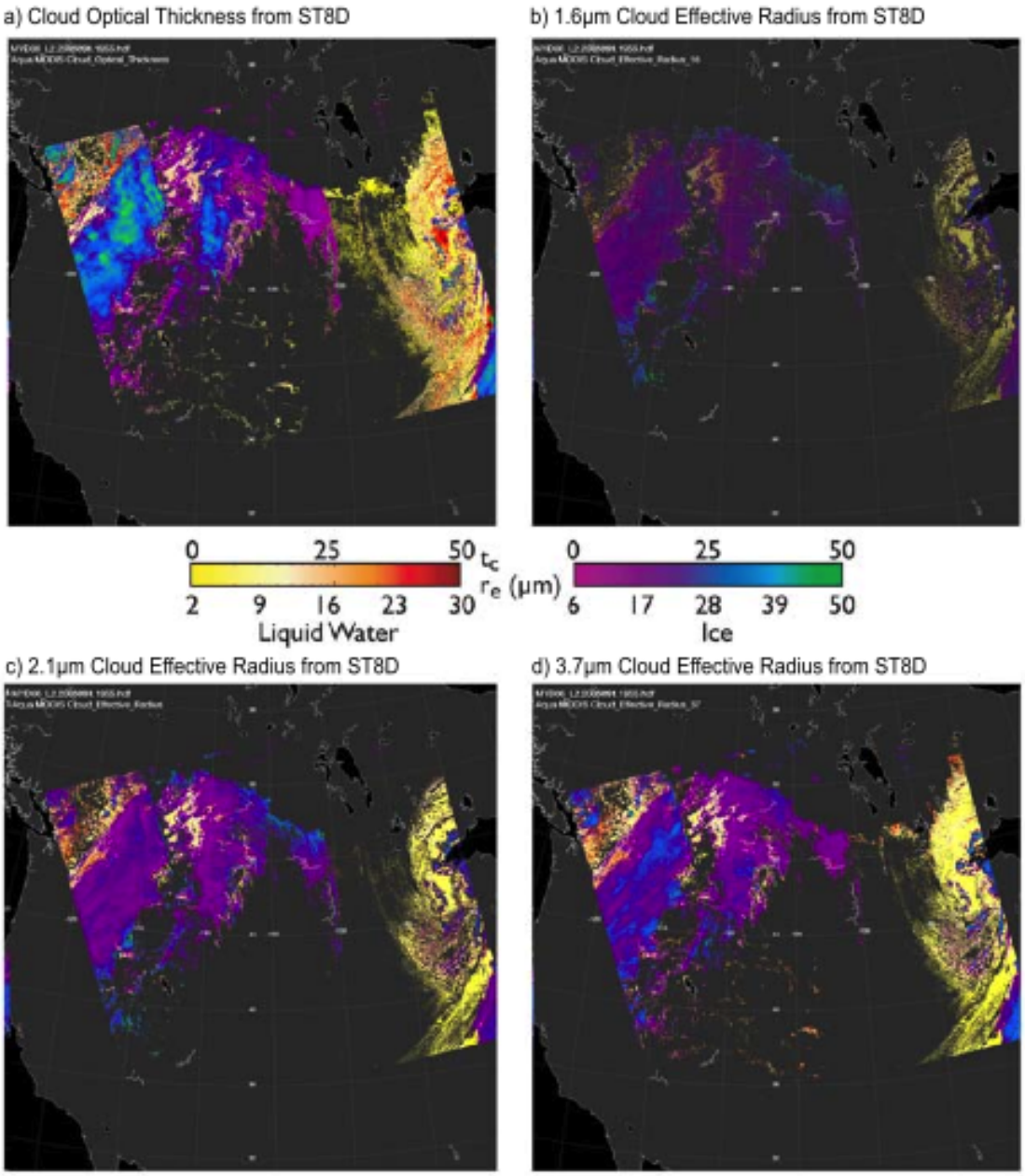

Figure 7: Aqua MODIS 2005 day 091, 19:55 UTC, Western United States. The panels illustrate new retrievals from ST8D as cloud optical thickness in panel a), 1.6 μm cloud effective radius in panel b), 2.1 μm cloud effective radius in panel c) and 3.7 μm cloud effective radius in panel d).

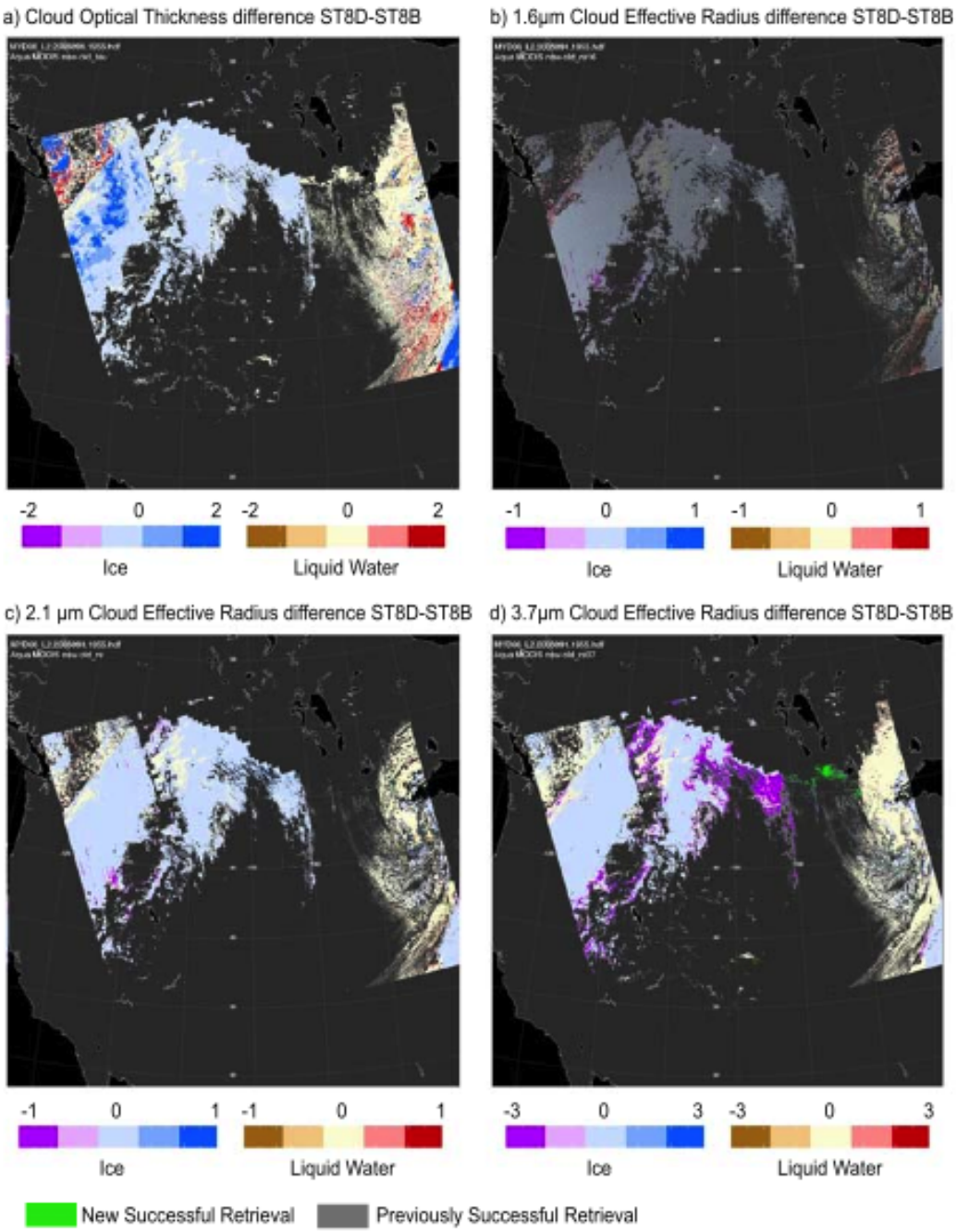

Figure 8: Aqua MODIS 2005 day 091, 19:55 UTC, Western United States. The panels illustrate differences between ST8D and ST8B as cloud optical thickness in panel a), 1.6 µm cloud effective radius in panel b), 2.1 µm cloud effective radius in panel c) and 3.7 µm cloud effective radius in panel d). New successful retrievals are shown in green and retrievals that previously succeeded but now fail are in medium gray.

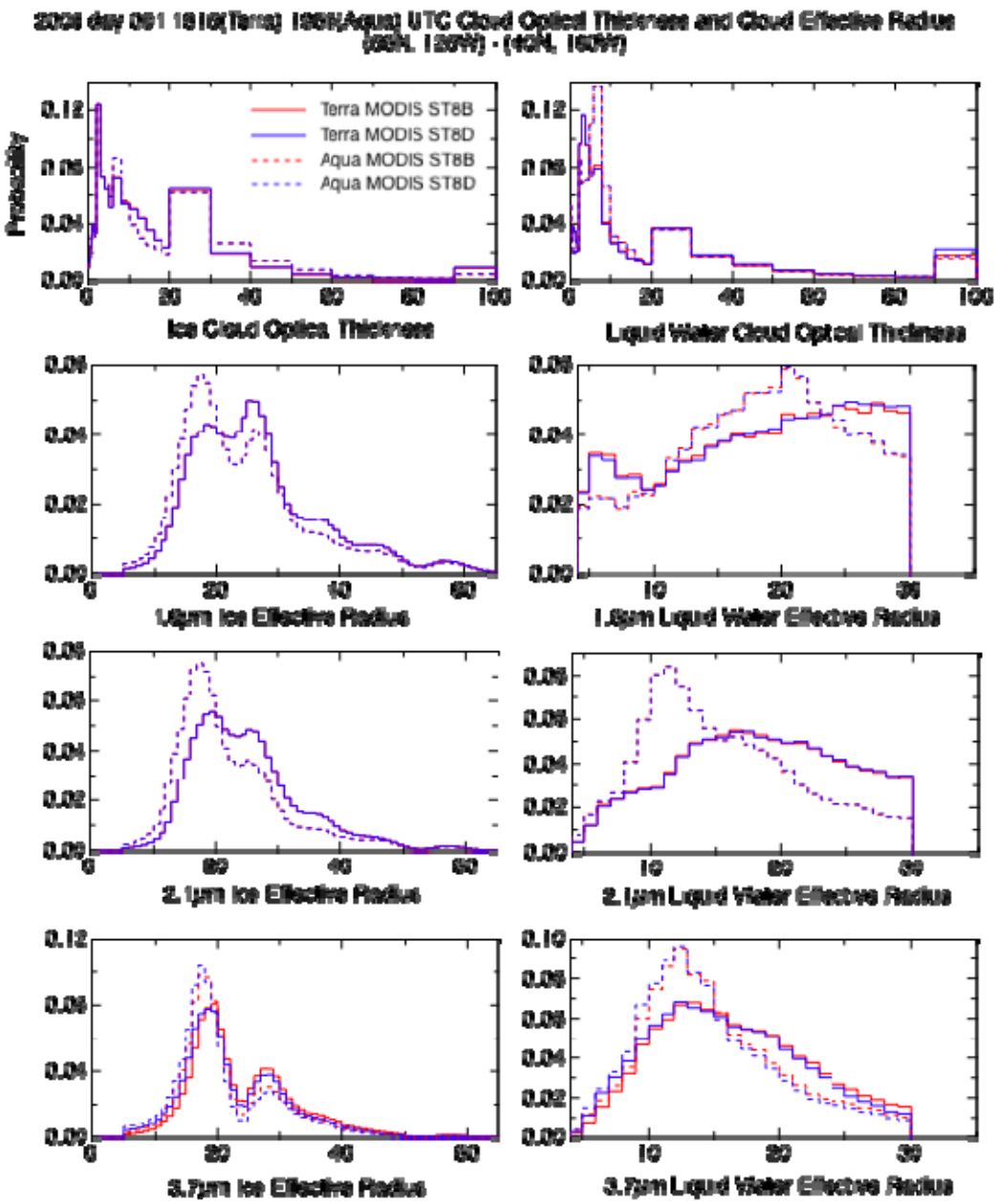

Figure 9: Histograms of retrieved optical thickness and 3.7 μm cloud effective radius for the Western US case.

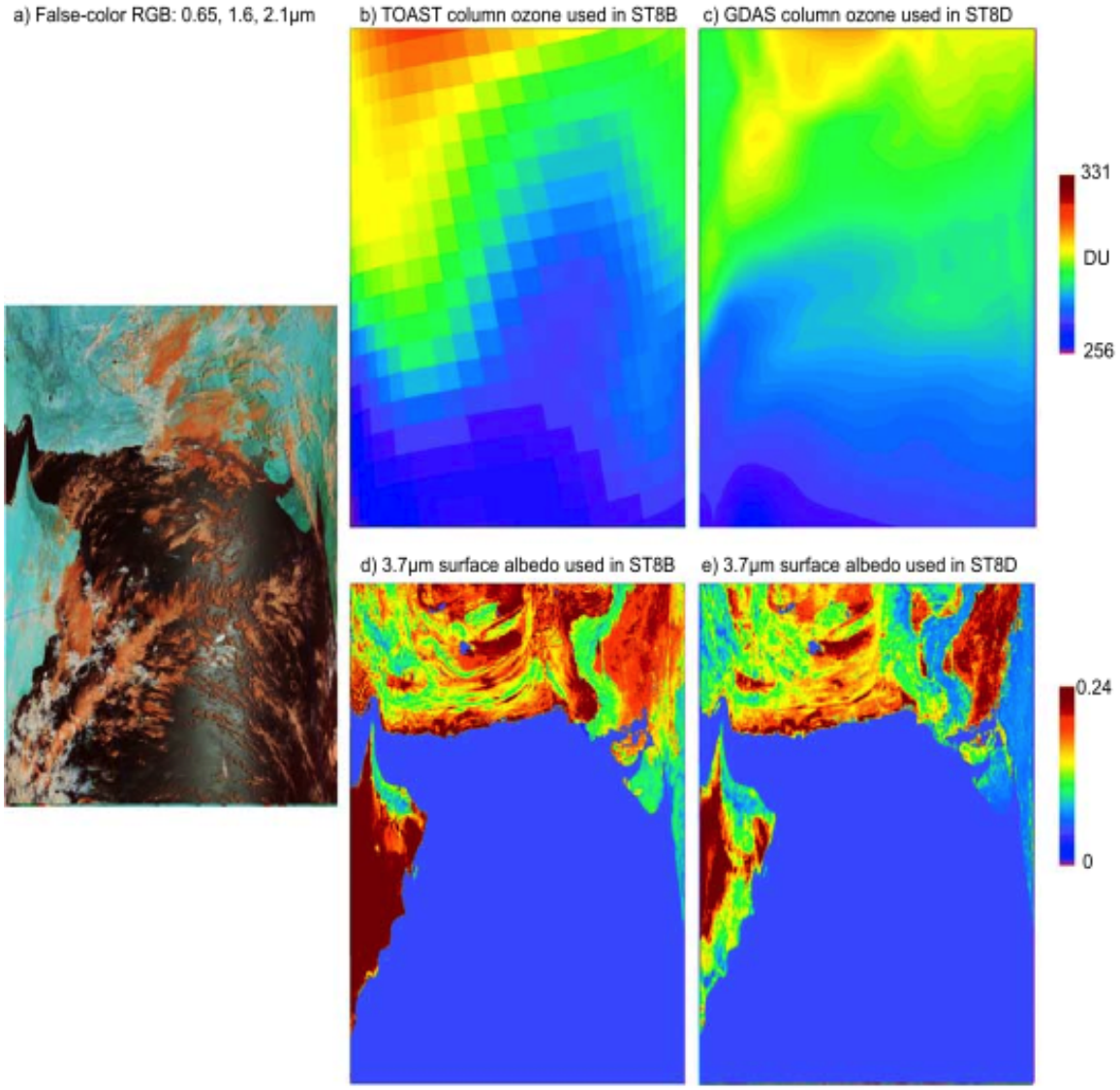

Figure 10: Terra MODIS 2005 day 111, 06:25 UTC. Panel a) shows the false-color RGB composite RGB: 0.65, 1.6, 2.1 μm. Panel b) shows the original column ozone field used in ST8B. Panel c) shows the new interpolated column ozone field. Panels d) and e) show 3.7 μm surface albedo for ST8B and ST8D respectively.

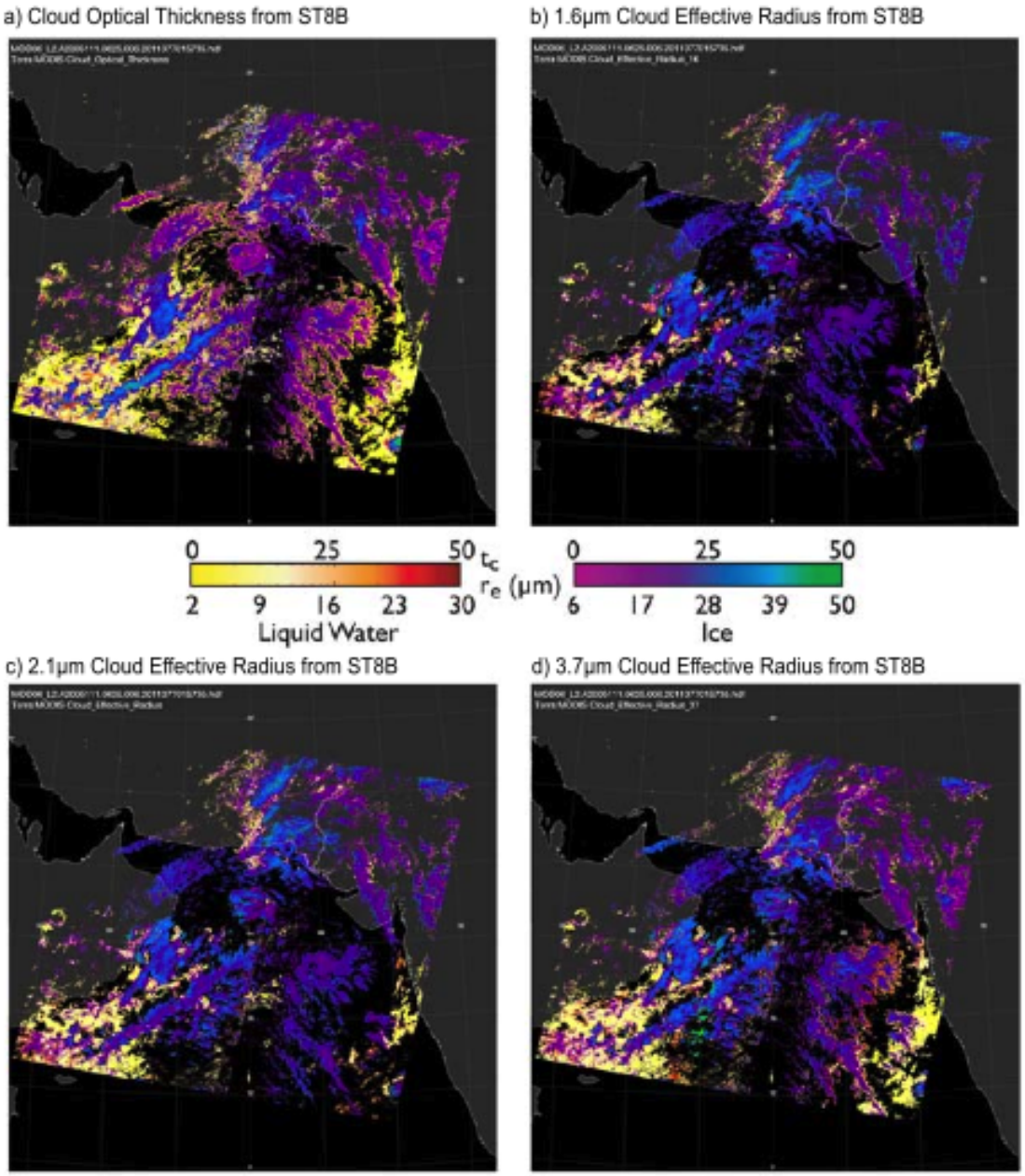

Figure 11: Terra MODIS 2005 day 111, 06:25 UTC, Northern Arabian Sea. The panels illustrate baseline retrievals from ST8B as cloud optical thickness in panel a), 1.6 μm cloud effective radius in panel b), 2.1 μm cloud effective radius in panel c) and 3.7 μm cloud effective radius in panel d).

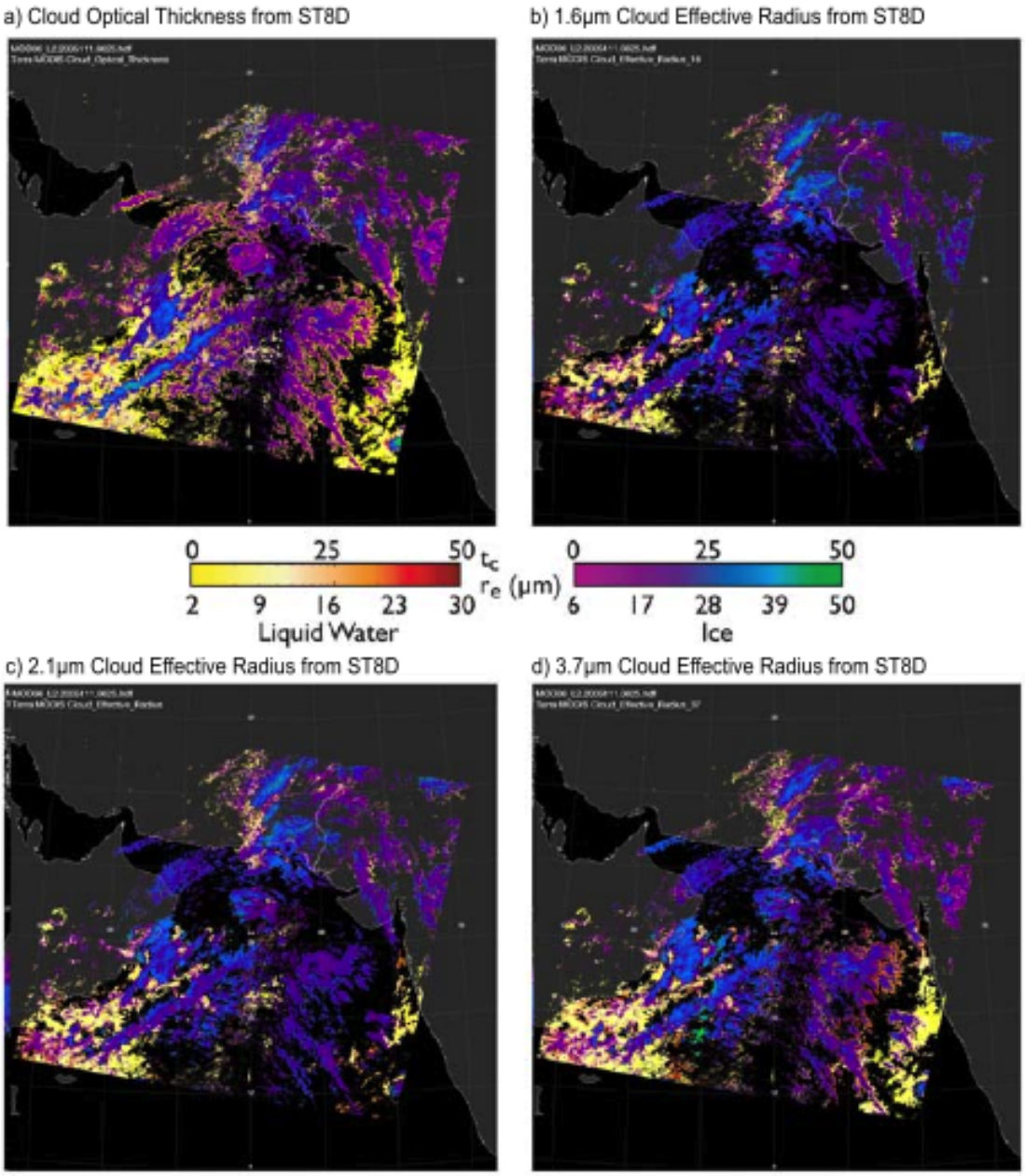

Figure 12: Terra MODIS 2005 day 111, 06:25 UTC, Northern Arabian Sea. The panels illustrate new retrievals from ST8D as cloud optical thickness in panel a), 1.6 μm cloud effective radius in panel b), 2.1 μm cloud effective radius in panel c) and 3.7 μm cloud effective radius in panel d).

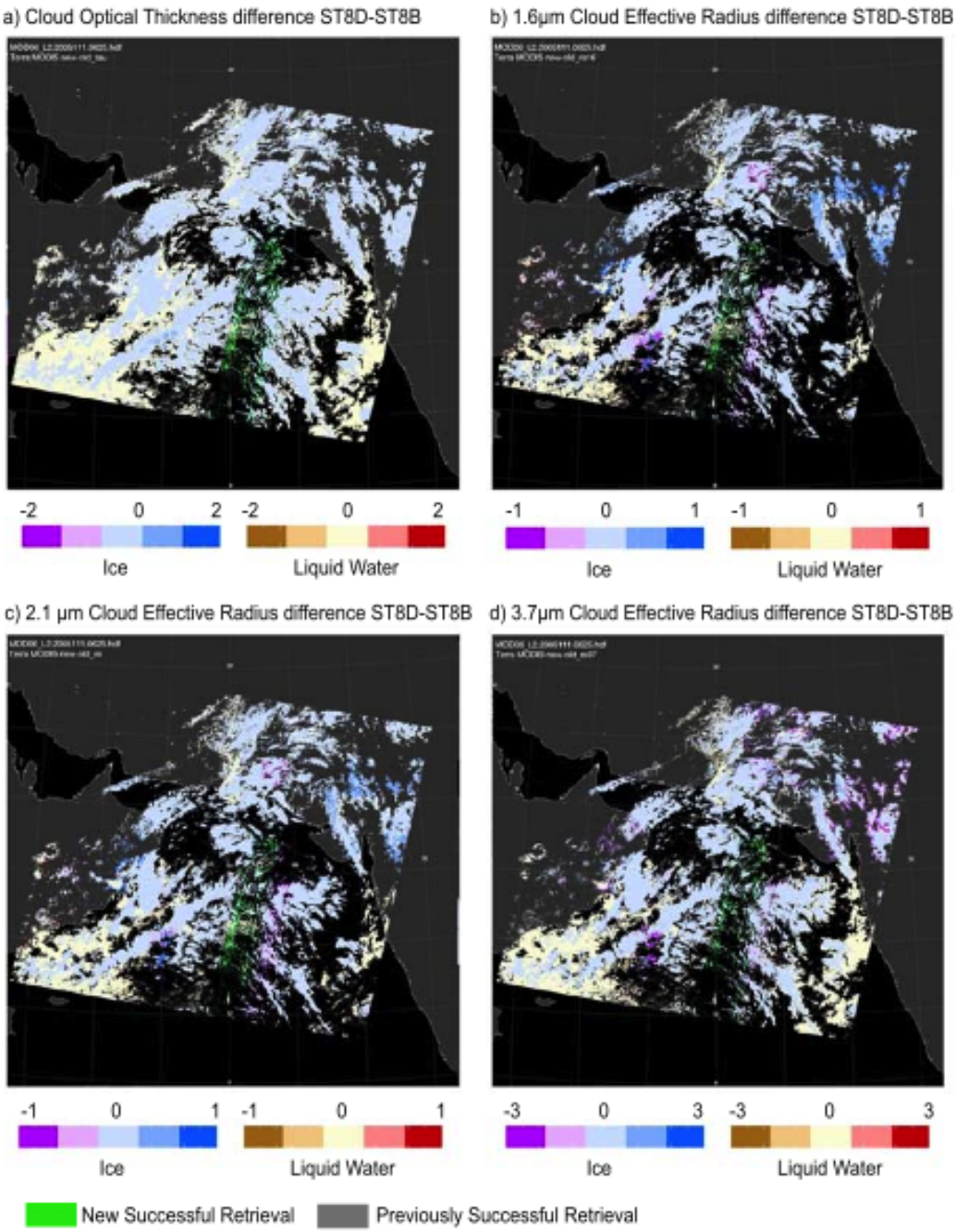

Figure 13: Terra MODIS 2005 day 111, 06:25 UTC, Northern Arabian Sea. The panels illustrate differences between ST8D and ST8B as cloud optical thickness in panel a), 1.6 μm cloud effective radius in panel b), 2.1 μm cloud effective radius in panel c) and 3.7 μm cloud effective radius in panel d). New successful retrievals are shown in green and retrievals that previously succeeded but now fail are in medium gray.

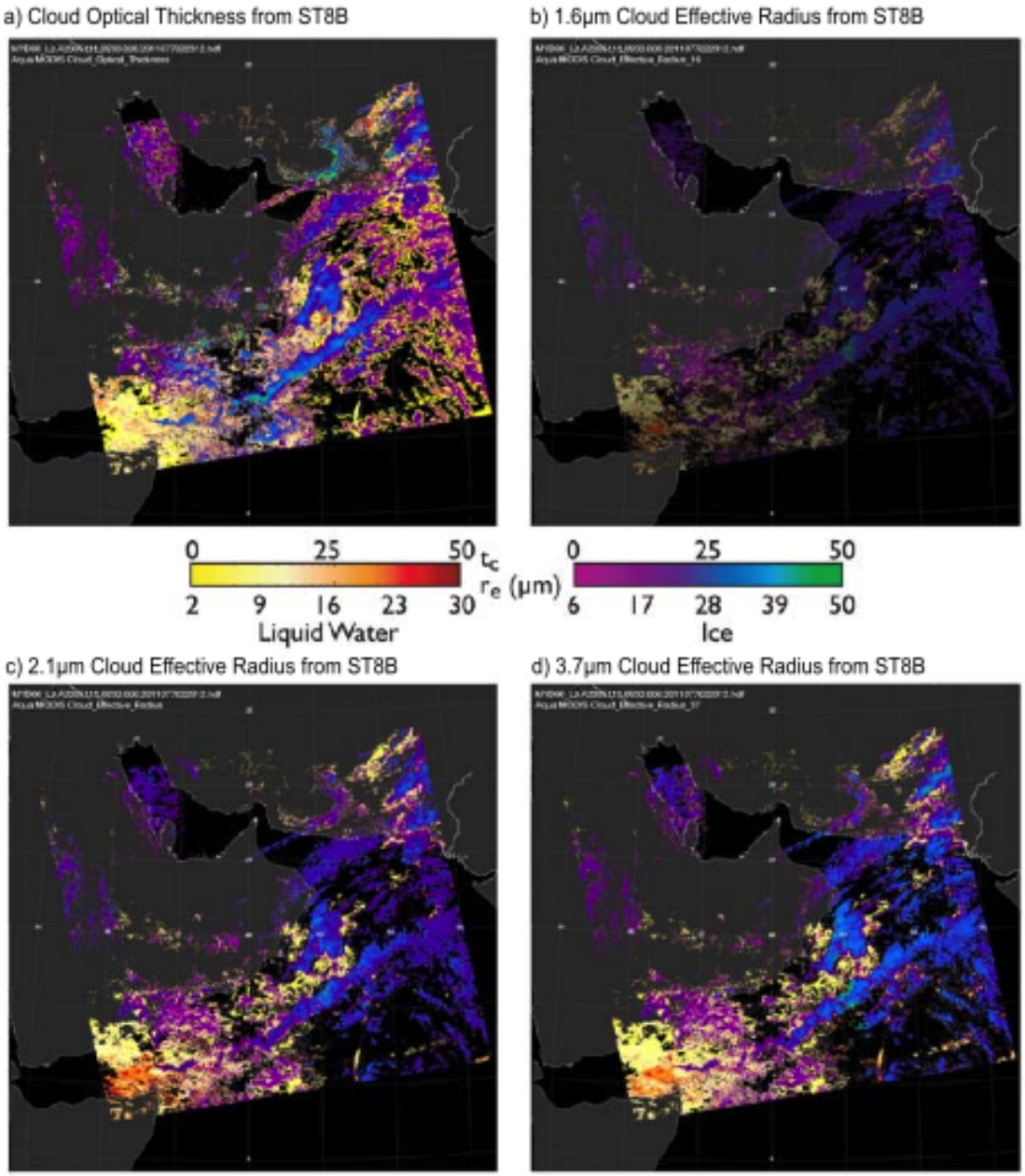

Figure 14: Aqua MODIS 2005 day 111, 09:30 UTC, Northern Arabian Sea. The panels illustrate baseline retrievals from ST8B as cloud optical thickness in panel a), 1.6 μm cloud effective radius in panel b), 2.1 μm cloud effective radius in panel c) and 3.7 μm cloud effective radius in panel d).

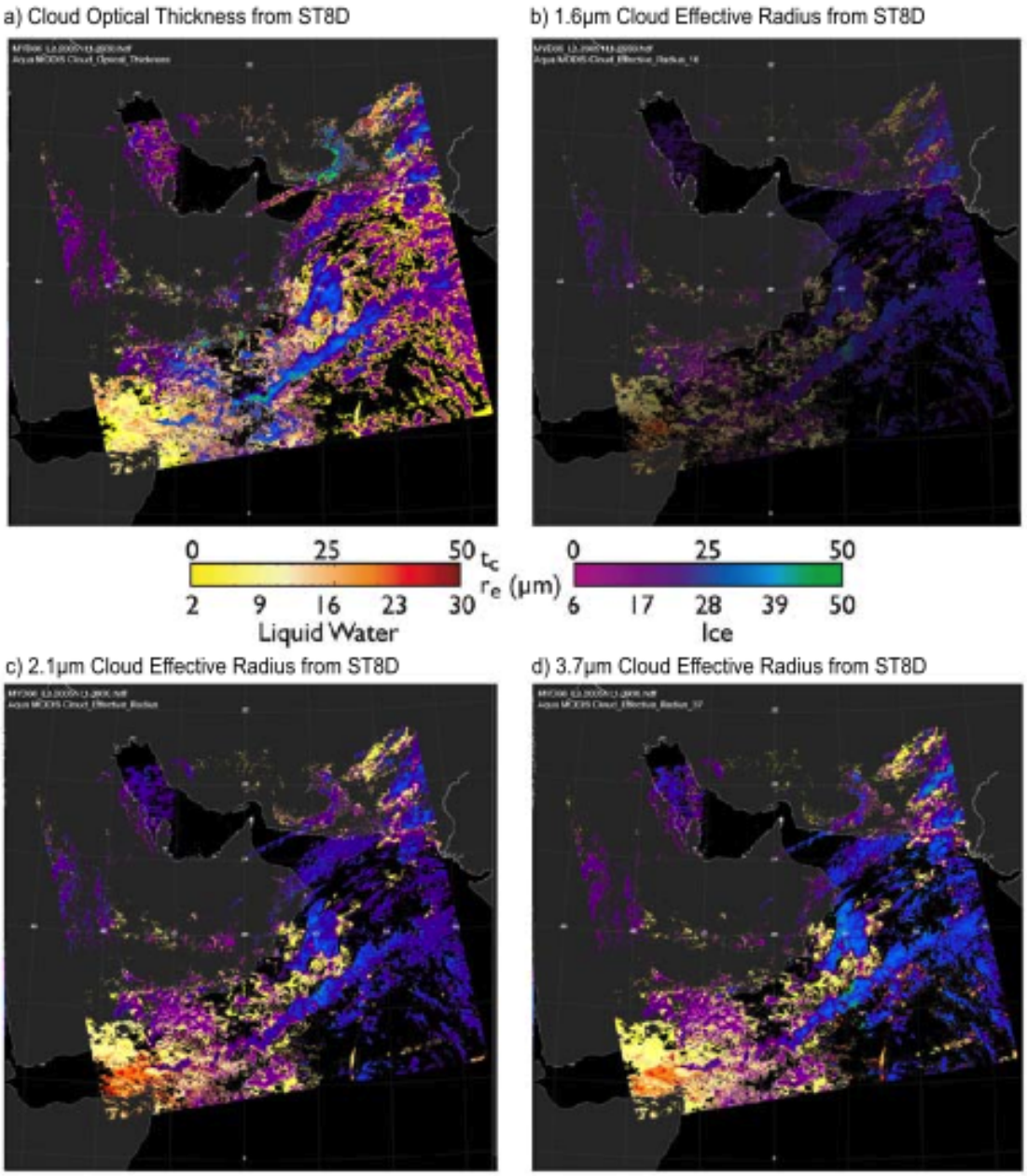

Figure 15: Aqua MODIS 2005 day 111, 09:30 UTC, Northern Arabian Sea. The panels illustrate new retrievals from ST8D as cloud optical thickness in panel a), 1.6 μm cloud effective radius in panel b), 2.1 μm cloud effective radius in panel c) and 3.7 μm cloud effective radius in panel d).

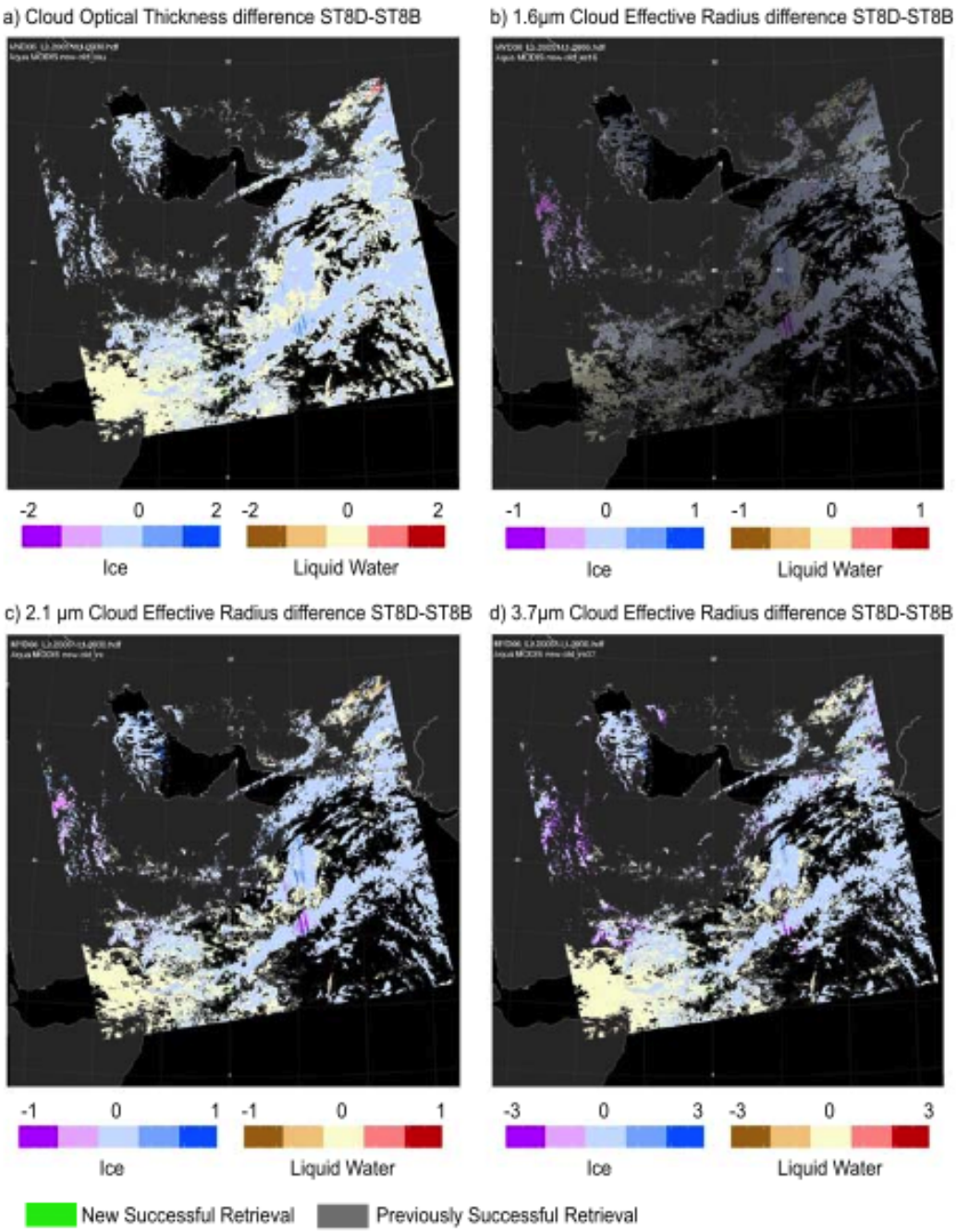

Figure 16: Aqua MODIS 2005 day 111, 09:30 UTC, Northern Arabian Sea. The panels illustrate differences between ST8D and ST8B as cloud optical thickness in panel a), 1.6 μm cloud effective radius in panel b), 2.1 μm cloud effective radius in panel c) and 3.7 μm cloud effective radius in panel d). New successful retrievals are shown in green and retrievals that previously succeeded but now fail are in medium gray.

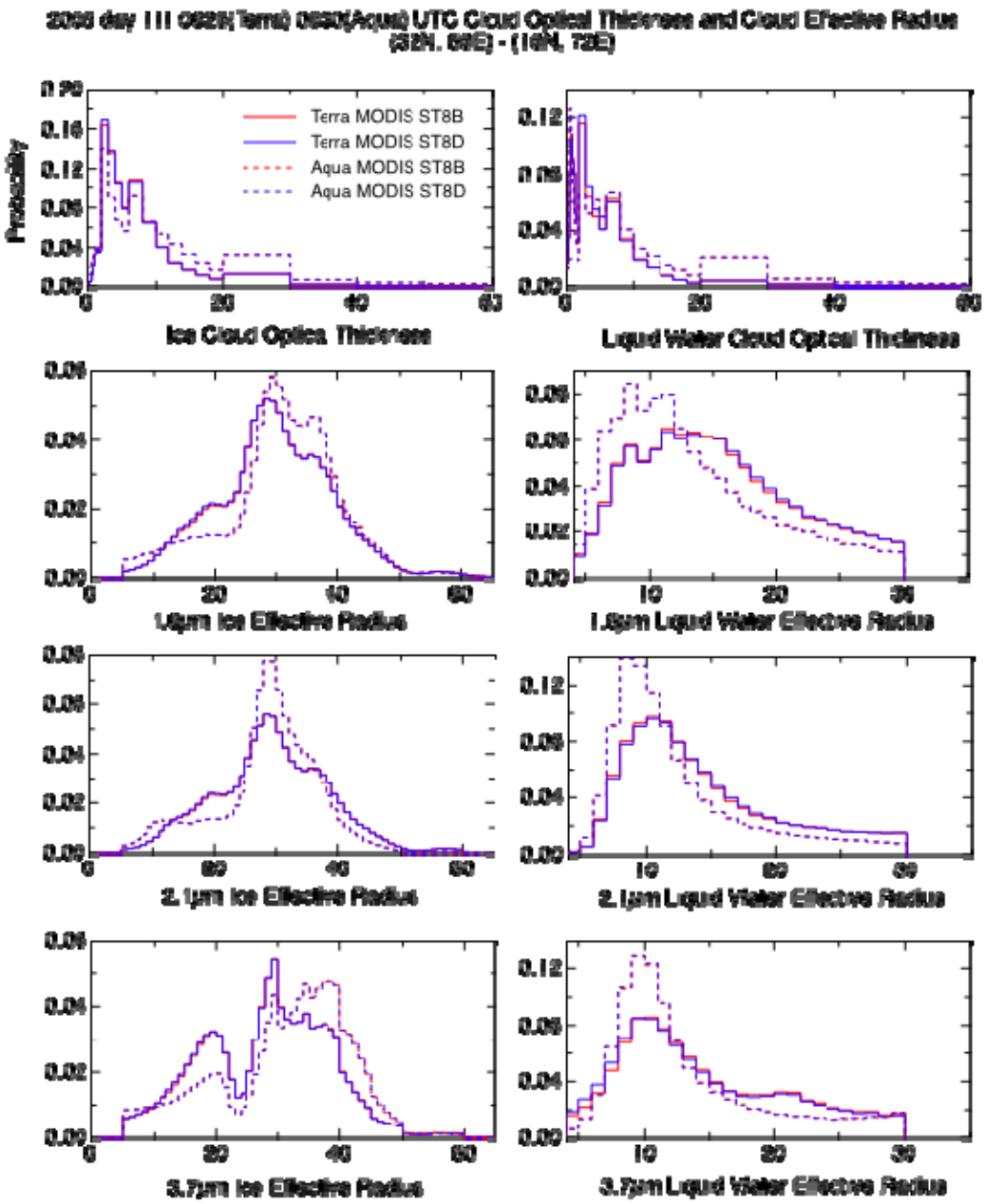

Figure 17: Histograms of retrieved optical thickness and cloud effective radius for the Arabian Sea case.